Partial Structure Factors in 1,4-Polybutadiene. A Combined Neutron Scattering and Molecular Dynamics Simulations Study

A. Narros,[†] A. Arbe,[*,‡] F. Alvarez,[†,‡] J. Colmenero,[†,‡,§] R. Zorn,[⊥] W. Schweika,[⊥] and D. Richter[⊥]

Departamento de Física de Materiales, UPV/EHU, Apartado 1072, 20080 San Sebastián, Spain; Unidad Física de Materiales (CSIC−UPV/EHU), Apartado 1072, 20080 San Sebastian, Spain; Donostia International Physics Center, Paseo Manuel de Lardizabal 4, 20018 San Sebastian, Spain; and Institut für Festkörperforschung, Forschungszentrum Jülich GmbH, D-52425 Jülich, Germany

Received July 6, 2005; Revised Manuscript Received September 20, 2005

ABSTRACT: We have investigated the short-range order in 1,4-polybutadiene by combining fully atomistic MD simulations and neutron diffraction with polarization analysis on isotopically labeled samples. Thereby the structure factor corresponding to the fully deuterated sample and the partial structure factor of the fully protonated polymer have been obtained. Both functions show a first main peak centered at about 1.4 $Å^{-1}$ and a second one at around 3 $Å^{-1}$. With varying temperature, we observe opposite tendencies for the intensity of the first diffraction peak in each sample. The direct comparison between simulation and experimental data has allowed validation of our simulated cell. Exploiting the information on the simulations, we have found that CC correlations dominate the first diffraction peak for both the deuterated and the protonated samples, while the origin of the second maximum depends on the labeling. Finally, the temperature behavior of the first peaks has also been rationalized. To a large extent, density changes are driving the evolution of the peaks, and the way they affect mainly the CC correlations and the mixed correlations involving C and H determines the behavior observed in the diffraction patterns.

I. Introduction

The short-range order of polymer melts and glassy polymers is still poorly understood. Information on this structural property is revealed by the static structure factor $S(Q)$ and the Fourier transform of the radial distribution function $g(r)$. For samples composed of carbons and hydrogens, $S(Q)$ can be directly measured by neutron diffraction using a fully deuterated sample—as the neutron scattering lengths of carbon and deuteron are very similar, both atoms are almost indistinguishable for neutrons. The effects of short-range order in polymers become apparent at $Q \gtrsim 0.5$ $Å^{-1}$. $S(Q)$ shows marked—though rather broad—diffraction maxima at Q values between 1 and 2 $Å^{-1}$ and weaker maxima at higher values, about 3 $Å^{-1}$. While the latter are attributed to mainly intra-macromolecular correlations, the peaks in the region below ≈2.5 $Å^{-1}$ are thought to be of intermolecular nature (see, e.g., ref 1). However, almost nothing is known about the relationship between these maxima and the particular chemical structure of the monomer or the microstructure of the chain. For instance, some polymers such as polyethylene,[2] 1,4-polybutadiene,[1,3,4] poly(ethylene propylene),[5] poly(ethylene oxide),[6] polyisobutylene,[7] or poly(vinyl chloride)[8] show only one main peak in the intermolecular region while others display a peak with a shoulder or even two clearly distinguished peaks as, e.g., polyisoprene,[9,10] polystyrene,[11,12] polycarbonate,[13,14] or 1,2-polybutadiene.[15] It is noteworthy that the presence of such shoulders or second peaks in the intermolecular range of Q is not always correlated with the existence of a bulky side group in the monomer, as could be expected from simple arguments.

In the case of complicated molecular systems such as polymers, the average structural information contained in either $g(r)$ or $S(Q)$ does not allow to unveil the short range order details. Fortunately, additional and complementary experimental information on the particular correlations arising from groups of selected atoms can be achieved by the study of partial static structure factors. These can be accessed by using e.g. X-rays and/or neutron diffraction combined with isotopic substitution techniques. The very different neutron scattering lengths of hydrogen and deuteron atoms allow selectively highlighting certain atomic pair correlations. Moreover, with the help of polarization analysis of the diffracted neutrons, the coherent contribution to the scattering can be determined at an absolute scale. However, the final interpretation of the experimental results in terms of the atomic correlations is usually extremely difficult.

The development of modern computer simulation techniques has provided a new route to answer the question of the short-range order in complex systems. In particular, the tandem composed by fully atomistic molecular dynamics (MD) simulations and diffraction measurements revealing the partial structure factors on real samples has proven to be the most promising tool for unraveling the local structure of polymer melts. Simulation enables precise insight into the atomic structure and allows an easy and controlled variation of the "experimental" conditions. However, fully atomistic and realistic samples are necessary; i.e., first of all, the simulated cells have to be validated by comparison with experimental data. Naturally, the most critical check of the structural resembling of the simulated cell and the real system can be achieved by comparing the largest possible number of partial structure factors. To date, a coordinated effort in this line has been carried out in only a few cases: polycarbonate,[13] polystyrene,[11,12] and, recently, polyisoprene samples.[10]

[†] UPV/EHU.
[‡] CSIC−UPV/EHU.
[§] Donostia International Physics Center.
[⊥] Forschungszentrum Jülich GmbH.

10.1021/ma051466a CCC: $30.25
Published on Web 10/19/2005

1,4-Polybutadiene (1,4-PB) is one of the most extensively studied polymers. A large number of works have already been devoted to unveil the structure of this system by MD simulations. Some of them dealt with the particular microstructure where all units present the *cis* conformation (1,4-*cis*-PB).[16−18] From those works, comparison with published results on the structure factor from neutron diffraction on the fully deuterated sample[1] was done in a qualitative way in the case of Okada et al.,[17] while Tsolou et al.[18] directly compared their simulated results with the experimental data. It is worth noting that the microstructure of the real system as obtained by anionic polymerization contains also *trans* units and a few vinyl units, and therefore the structural validation of such model systems is not so straightforward. Simulations on 1,4-PB with microstructures closer to those of real samples were also carried out by Kim et al.,[19] though not direct comparison with experimental scattering data on the structure was performed. Also close to the real microstructure was that of the cell simulated by Bedrov et al.[20] by using a united atom model. In some of those works,[18−20] the inter- and intramolecular contributions to the structure factor were unraveled. Interestingly, the pressure dependence of the different correlations was also investigated by Bedrov et al.,[20] who found a qualitative agreement with the experimental results reported on the pressure dependence of the $S(Q)$ on deuterated samples.[4] However, no direct comparison with experimental data was shown in that work.

Trying to contribute to the understanding of the structural properties of 1,4-PB, in this work we have exploited the potential of the combination of fully atomistic MD simulations and neutron diffraction with polarization analysis on labeled samples. The microstructure of both simulated and real samples was nearly the same. From an experimental point of view, the main contribution of this work is that for the first time we present results on the partial structure factor corresponding to the fully protonated sample as a function of temperature. This has been investigated in a wide Q range covering the inter- and intra-macromolecular range, together with the $S(Q)$ from a fully deuterated sample. In parallel, the same functions have been calculated from fully atomistic MD simulations on this polymer. The excellent agreement found between both series of data has allowed us to exploit the information contained in the simulations and unveil the origin of the atomic correlations contributing to the diffraction peaks. Finally, we have determined the temperature and density effects on the different atomic correlations and their manifestations on the total and partial structure factors.

II. Experiments and Simulations

A. Samples. The two samples used in this investigation were linear polybutadienes synthesized by anionic polymerization.[21] The protonated material (1,4-PBh6) had a molecular weight M_w = 20 000 and a microstructure of 42% *cis*, 51% *trans*, and 7% vinyl monomeric units. The glass-transition temperature was T_g = 178 K determined by differential scanning calorimetry (DSC). The fully deuterated polybutadiene (1,4-PBd6) had the same microstructure, with M_w = 31 600 and a deuteration of 97.5% as determined from NMR. In both cases the polydispersity was lower than 1.02.

B. Neutron Scattering: Diffraction with Polarization Analysis. Neutron diffraction assesses the differential cross section, i.e., the number of scattered neutrons into a solid angle between Ω and $\Omega + d\Omega$, relative to the number of incident neutrons.[22−24] The modulus of the momentum transfer, Q, is determined by $Q = 4\pi \sin(\theta/2)/\lambda$, where θ is the scattering angle and λ the wavelength of the incoming neutrons. The differential cross section contains scattering of two natures: coherent and incoherent. The coherent contribution can be expressed as

$$\left(\frac{\partial\sigma}{\partial\Omega}\right)_{coh} = \frac{1}{N}\left\langle \sum_{i,j=1}^{N} \bar{b}_i \bar{b}_j e^{i\vec{Q}\vec{r}_{ij}} \right\rangle \quad (1)$$

where the $\bar{b}_i$ stand for the coherent scattering lengths for neutrons ($\bar{b}_H = -0.3741 \times 10^{-14}$ m; $\bar{b}_C = 0.6648 \times 10^{-14}$ m; $\bar{b}_D = 0.6674 \times 10^{-14}$ m) and N is the number of atoms. $\vec{r}_{ij} = \vec{r}_i - \vec{r}_j$ is the vector connecting atoms i and j at the same time, and the brackets denote the thermal average. The cross sections like σ_{coh} are given in units of barns/atom, and $(\partial\sigma/\partial\Omega)_{coh}$ is in units of barns/(sr atom) (1 barn = 10^{-28} m^2). The $Q \to \infty$ limit of the coherent differential cross section is determined by the coherent cross section σ_{coh}:

$$\lim_{Q\to\infty}\left(\frac{\partial\sigma}{\partial\Omega}\right)_{coh} = \frac{1}{N}\sum_{i=1}^{N}\bar{b}_i^{\,2} = \frac{\sigma_{coh}}{4\pi} \quad (2)$$

On the other hand, in an ideal case, the incoherent contribution to the differential cross section is Q-independent and given by the total incoherent cross section σ_{inc}:

$$\left(\frac{\partial\sigma}{\partial\Omega}\right)_{inc} = \frac{1}{4\pi N}\sum_{i=1}^{N}\sigma_{inc}^{i} = \frac{\sigma_{inc}}{4\pi} \quad (3)$$

(σ_{inc}^{H} = 80.27 barns; $\sigma_{inc}^{C} = 0$; σ_{inc}^{D} = 2.05 barns).

If the incoherent scattering arises solely from spin disorder, it flips the neutron spin with probability $^2/_3$, while coherent scattering leaves the spin unchanged. This allows to experimentally separate the coherent and incoherent contributions to the scattering by using a spin-polarized neutron beam and polarization analysis (see, e.g., refs 22 and 23). With the incident beam polarized, the number of neutrons scattered within a given solid angle with spin-flipped (SF) and non-spin-flipped (NSF) are

$$I_{SF} = A\frac{2}{3}\left(\frac{\partial\sigma}{\partial\Omega}\right)_{inc} \quad (4)$$

$$I_{NSF} = A\left[\left(\frac{\partial\sigma}{\partial\Omega}\right)_{coh} + \frac{1}{3}\left(\frac{\partial\sigma}{\partial\Omega}\right)_{inc}\right] \quad (5)$$

where A is a proportionality factor that depends on the experimental conditions (amount of sample in the beam, primary beam intensity, detector efficiencies, etc.). In the absence of inelasticity and multiple scattering, the value of A can easily be obtained from the SF measurement and the simple calculation of σ_{inc}; then, the partial structure factor can be determined in a straightforward way from the NSF measurement in absolute units.

On the basis of this principle, in this work, we used the diffuse scattering spectrometer DNS at Jülich, in its diffraction mode. This instrument is equipped with a horizontally and vertically focusing monochromator, and a wide angular range around the sample is covered with detectors. Incident neutrons can be polarized by a focusing bender assembled by a stack of supermirrors. A detector bench with 12 detector units is equipped with similar benders for polarization analysis. For spin-flip measurements a Mezei-type flipper is installed in the incident beam. The incident wavelength was set to 3.3 Å, enabling a range of scattering vectors Q up to 3.34 Å^{-1}. Since $S(Q)$ for 1,4-PBd6 has already been thoroughly studied in previous works,[1,3,4] we have restricted our measurements on this sample to 200 and 280 K and focused on the novel protonated sample. For this, the experiments were performed at 10, 160, 200, and 280 K. Both samples were put as films

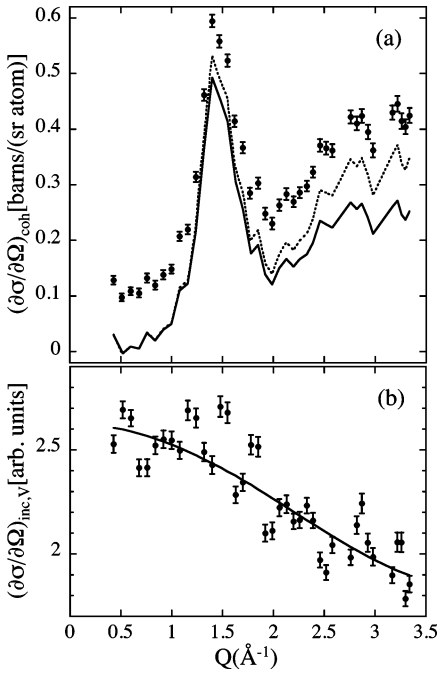

Figure 1. (a) Differential coherent neutron cross section of 1,4-PBh6 at 200 K from DNS. The full symbols with error bars show the raw data from inversion of eqs 4 and 5. The dashed curve represents data after multiple scattering correction. The continuous curve shows the final data treatment stage after the inelasticity correction. (b) Vanadium normalized differential incoherent neutron cross section from the same sample. The curve is a fit with a biquadratic polynomial.

into a hollow cylindrical aluminum sample holder of 10 mm diameter. For each Q value, spin-flip and non-spin-flip measurements were of 22 min for PBh6 and 16 min in the case of PBd6. The correction for background scattering was done by the measurement of the scattering from the empty cell. The corrections for multiple scattering and inelasticity have been done in the same way as in ref 10: It was assumed that for the second and following orders the scattering probability is constant and the scattering is isotropic. Under this assumption the total scattering can be expressed as a geometric series of scattering orders. This series can be summed up analytically and inverted to obtain the single scattering cross section.[25] The effect of this correction is shown exemplarily as the dashed curve in Figure 1a. The inelasticity was corrected by an empirical correction. In the absence of inelasticity the incoherent neutron scattering cross section $(\partial\sigma/\partial\Omega)_{inc}$ should be independent of Q. The actually measured $(\partial\sigma/\partial\Omega)_{inc}$ can be obtained from the same experiment using eq 4 and comparing it with the known incoherent scattering from a vanadium standard. The deviation was fitted by a biquadratic expression $C(1 + aQ^2 + bQ^4)$ to reduce statistical errors (Figure 1b). The thus-obtained factor $(1 + aQ^2 + bQ^4)$ was then used to correct the coherent scattering for inelasticity (continuous curve in Figure 1a).

C. Molecular Dynamics Simulations: Method. The simulations were carried out by using the Insight (Insight II 4.0.0 P version) and the Discover-3 module from Molecular Simulations Inc. (now Accelrys) with the Polymer Consortium Force Field (PCFF). More information about this kind of force field, including the complete analytical expression for the functional form, can be found in refs 26−29. A cubic cell containing one polymer chain of 130 monomers was constructed at 280 K by means of the amorphous cell protocol[30,31] with periodic boundary conditions. The microstructure of the chain (53% *trans*, 39% *cis*, and 8% vinyl units) was built to be similar to that studied by neutron scattering. By means of NPT (keeping constant the number of atoms, the pressure, and the temperature of the cell) dynamic runs, the equilibrium density was found to be 0.835 g/cm^3, which leads to a cell side value of 24.095 Å. After this procedure, the energy of the structure was minimized (Polak-Ribiere conjugate gradient method), and the system was dynamically equilibrated by a dynamic run of 1 ns in NVT (keeping constant the number of atoms, the volume, and the temperature of the cell) conditions. The chosen temperature was high enough (T_g + 100 K) to allow local structural equilibration of the sample in this time. The system obtained in this way was used as a starting point for collecting data every 0.01 ps during a MD run of 1 ns. As an integration method we have used the velocity-Verlet algorithm with a time step of 1 fs. To control the temperature, instead of a real temperature bath coupling (Nose-Hoover or Berendsen thermostats, for instance), we have followed a rather crude velocity scaling procedure but with a wide temperature window of 10 K. Under these conditions, greater temperature fluctuations are allowed but the trajectory is disturbed less. In fact, we have checked that by following this simple procedure we obtain results similar to those obtained with a NVE ensemble (by keeping constant the sample total energy instead of its temperature), which has the proper Newtonian dynamics. After the first collecting data 1 ns MD run, two more successive runs of 2 and 20 ns were carried out, collecting data every 0.05 and 0.5 ps, respectively. Nearly indistinguishable results were obtained from the different simulation runs.

Starting from the equilibrated cell at 280 K, the temperature was gradually lowered to 200 K by a series of NPT dynamics steps at atmospheric pressure. Once the equilibrium density at 200 K was reached (0.879 g/cm^3), the energy of the structure was once again equilibrated at this temperature, and the system was dynamically equilibrated in the NVT ensemble. Because of the low temperature simulated ($\approx T_g$ + 20 K), the duration of the equilibrium run was in this case very long (100 ns). A subsequent NVT run of again 160 ns was used to produce the MD simulation data. A further run of 300 ns confirmed the absence of aging phenomena affecting the data. A comparison of the dynamic structure factor $S(Q,t)$ obtained from the simulations with real neutron spin-echo measurements[32] showed a rather good agreement, which validates the simulation even at this low temperature.

On the other hand, to unravel the effects of density and temperature on the structure factor, we have carried out additional MD simulation runs at the following conditions. First, we have kept constant the equilibrium density corresponding to 200 K, i.e., the volume in NVT conditions, and then, the temperature was increased to 280 K. A simulation scheme for collecting data similar to that above described was followed at these conditions. The same procedure was also repeated but now keeping constant the equilibrium density (volume) at 280 K and decreasing the temperature to 200 K.

Starting from the MD simulation results at the different conditions, we have calculated the coherent differential cross section $(\partial\sigma/\partial\Omega)_{coh}$ for the two samples investigated. For an isotropic system and taking the orientational averaging, the coherent contribution can be written as

$$\left(\frac{\partial\sigma}{\partial\Omega}\right)_{coh} = \frac{1}{N}\left\langle \sum_{i,j=1}^{N} \bar{b}_i \bar{b}_j \frac{\sin(Qr_{ij})}{Qr_{ij}} \right\rangle \qquad (6)$$

In each case, $(\partial\sigma/\partial\Omega)_{coh}$ is calculated from the atomic coordinates of the corresponding simulation run by means of this equation and averaging it for a large number of frames throughout the atomic trajectories.

III. Results

The experimental results obtained for the two samples are displayed in Figure 2, where we can appreciate the very good quality of the DNS data. The structure factor obtained from the fully deuterated sample 1,4-PBd6 (Figure 2a) presents a first main peak—the so-called amorphous halo—centered at a Q value of about 1.45 Å^{-1}. As it has been reported[1,3] and can be seen in this figure, in the supercooled liquid regime this maximum

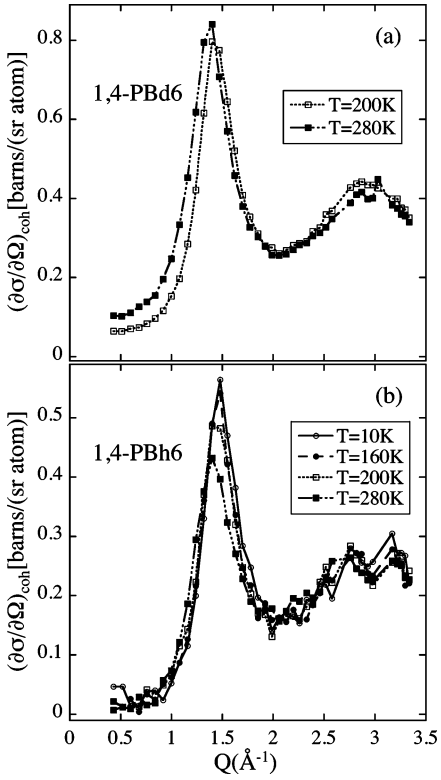

Figure 2. Coherent contribution to the neutron scattering as determined by DNS for the fully deuterated (a) and fully protonated (b) 1,4-PB samples at the temperatures indicated.

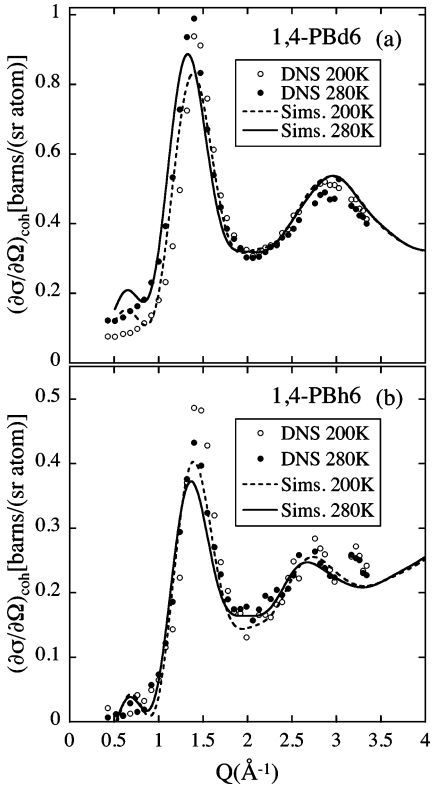

Figure 3. Comparison between the coherent contribution to the neutron scattering as determined by DNS (symbols) and by the MD simulations (lines) for the fully deuterated (a) and fully protonated (b) 1,4-PB samples at the temperatures indicated.

shifts toward lower Q values while its intensity increases with increasing temperature. The main changes affect the low-Q flank, while the high-Q flank remains almost unaltered. A second broad peak centered at about 3 Å^{-1} can also be observed. We note that in the Q region around 3 Å^{-1} aluminum Bragg peaks are present, the subtraction of which is rather difficult, especially for weakly coherently scattering samples. Therefore, a clear dependence of the intensity or position of this peak with temperature cannot be claimed. These results agree with previous diffraction measurements carried out on 1,4-PBd6 in a wider temperature range.[1,3] A qualitatively similar pattern is revealed by the partial structure factor of the fully protonated sample 1,4-PBh6 (Figure 2b). In the glassy state, the first peak is hardly T-dependent and centered at a Q value slightly below 1.5 Å^{-1}. Above the glass transition, with increasing temperature this peak shifts toward lower Q values—like the first maximum of $S(Q)$. However, contrary to the case of the deuterated sample, the tendency of the first peak obtained from 1,4-PBh6 is to decrease in intensity upon heating. In fact, in this case we observe that it is the high-Q flank that changes with temperature, whereas the low-Q flank hardly varies. Concerning the second peak, centered like that in $S(Q)$ at about 3 Å^{-1}, it does not show any significant temperature dependence, taking into account the uncertainties involved in the aluminum scattering subtraction. Finally, we note that globally the coherent intensity of the deuterated sample amounts to about 2 times that of the protonated sample.

Figure 3 shows the comparison between the coherent intensities obtained from the DNS experiments and from the MD-simulations. For the two samples investigated we observe a good agreement between both sets of data, taking into account that we are showing the data on an absolute scale. It is also noteworthy that not only the general features of the diffraction patterns but also their temperature dependences are very well reproduced by the simulations: the opposite behavior of the main peak intensity in both structure factors is perfectly mimicked by the simulated data.

IV. Discussion

Figure 2 shows that, apart from the absolute values, the coherent intensities corresponding to the two samples measured, 1,4-PBd6 and 1,4-PBh6, are very similar, showing only one well-defined peak in the so-called intermolecular Q range. As it has already been mentioned, in the case of 1,4-PBd6 all atomic pair correlations are weighted in the same way due to the nearly identical values of the coherent scattering lengths of carbon and deuteron. However, taking into account the coherent scattering length of hydrogen atoms, as well as previous results in other polymers, we can expect that the coherent intensity corresponding to 1,4-PBh6 is dominated by carbon−carbon correlations. The fact that the coherent intensity of the two samples displays a qualitatively similar peak suggests that all atomic pair correlations have a maximum at about the same Q value. This indicates some kind of regular packing which is not present in other simple polymers as, for instance, polyisoprene.[10] Another interesting experimental feature is the temperature dependence of the coherent intensity measured, which has already been described in the preceding section. The behavior displayed by 1,4-PBh6 is what is expected from the temperature dependence of the intermolecular correlations in glass-forming materials: a shift to lower Q values and a reduction in intensity with increasing

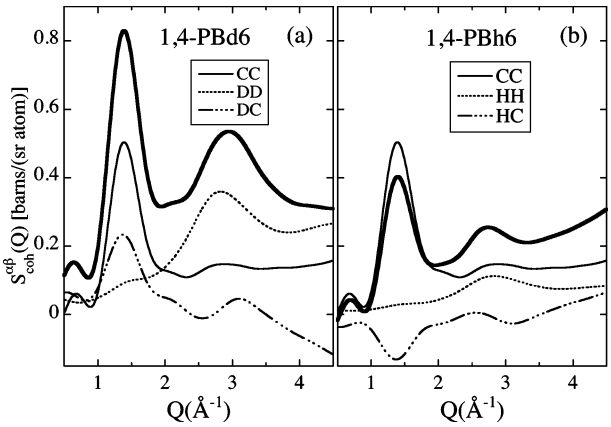

Figure 4. Contributions coming from the different atomic correlations to the coherent differential scattering cross sections (thick lines) of the fully deuterated (a) and fully protonated (b) 1,4-PB samples obtained from the MD simulations at 200 K.

temperature. On the other hand, the fully deuterated sample, 1,4-PBd6, shows just the opposite behavior, apparently suggesting enhanced structure at higher temperatures. However, the different temperature behavior found in the case of 1,4-PBh6 rather indicates that this anomalous temperature dependence is likely due to a complicated interplay among different atomic correlations. A similar situation was found in the case of polyisoprene.[10] In the following we will exploit the simulation capabilities to understand these features in a quantitative way.

From the above direct comparison of the MD simulation results with the experimental data, we can conclude that the inter- and intra-macromolecular structure obtained in our simulation cell constitutes a quite reasonable representation of the actual structure of polybutadiene. It is worth mentioning that not only the structural features but also the dynamical behavior is fairly well reproduced: an excellent agreement between experiment (neutron spin echo, NSE) and simulations is found for the dynamic structure factor and the self-correlation function of hydrogens.[32] Once thoroughly validated, we can take advantage of the information contained in the simulation data and try to identify the main atomic correlations contributing to the peaks. To do this, we have to consider separately the different atomic correlations in the simulated cell. Therefore, we have calculated the set of partial radial distribution functions $G_{CC}(r)$, $G_{HH}(r)$, and $G_{CH}(r)$ where C and H denote carbon and hydrogen, respectively. As our main interest is to unravel the different atomic correlations contributing to the peaks of the diffraction patterns, we will discuss our results in the reciprocal Q-space instead of the more customary real space. Therefore, we will consider the Fourier transform of $G_{\alpha\beta}(r)$, $A_{\alpha\beta}(Q)$ (α, β: C, H). These contributions are highlighted or downgraded in each sample according to the different neutron scattering lengths, so that the contribution of each atomic pair $\{\alpha,\beta\}$ to the coherent differential cross section is given by $S^{\alpha\beta}_{coh}(Q) = \bar{b}_\alpha \bar{b}_\beta A_{\alpha\beta}(Q)$. Of course, in the case of the deuterated sample the scattering length of hydrogen $\bar{b}_H$ in this expression has to be replaced by that of deuterium, $\bar{b}_D$.

Figure 4 shows all these contributions calculated from the simulations at 200 K for the two samples investigated. Of course, the CC contribution is the same for both labelings. As mentioned above, as $\bar{b}_C \cong \bar{b}_D$, the three contributions in the deuterated sample (CC, DD, DC) are equally weighted. For the protonated sample, however, the HH contribution is reduced by $^1/_3$ with respect to its DD counterpart in 1,4PBd6, and because of the negative value of $\bar{b}_H$, the cross-term involving carbons and hydrogens becomes negative in the region below $\approx$3.5 Å^{-1}.

At 200 K, as can be seen in Figure 4a, the correlation functions $A_{CC}(Q)$ and $A_{CH}(Q)$ show a maximum in the region of $Q \approx 1.4$ Å^{-1}. This is very pronounced in the CC correlations and much weaker for those involving carbons and hydrogens. A shoulder in this region is also present in the $A_{HH}(Q)$ function. These observations allow to conclude that to the first peak of $S(Q)$ all atomic pair correlations contribute constructively, but it is clearly dominated by the CC correlations and, in second place, by the cross-correlations involving C and H. At higher Q values, the main feature is shown by the HH correlations, with an intense peak close to 3 Å^{-1}. This is certainly the main origin of the second maximum in $S(Q)$ for 1,4-PB. We comment that a similar situation was found for polyisoprene (CC correlations dominate the first peak of $S(Q)$, while HH correlations are responsible for that at $\approx$3 Å^{-1}). Moving to the protonated sample (Figure 4b), we can see that the negative contribution of the $S^{HC}_{coh}(Q)$ term to the first peak—the maximum in A_{HC} close to $Q \approx 1.4$ Å^{-1} becomes a minimum for this sample—leads to a much weaker first peak than that observed in $S(Q)$. On the other hand, the intensity of the peak at $\approx$3 Å^{-1} is almost equally due to CC and HH correlations in this case. At this qualitative level, all these observations are similar for the other temperature investigated.

Once the origin of the peaks has been identified, we can now try to understand also the temperature dependences observed for the coherent intensities. Under the experimental conditions (constant pressure), a change in temperature involves also a change in the density of the sample. How does the change of each variable, temperature and density, influence the evolution of the peaks in the coherent scattering? To answer this question, we have calculated the temperature and density dependences of the different contributions $S^{\alpha\beta}_{coh}(Q)$. Figure 5 shows the results for the deuterated sample. In Figure 5a, the density has been kept constant to that in equilibrium at 200 K and atmospheric pressure and the temperature has been increased from 200 K (solid lines) to 280 K (dotted lines). As can be seen, at constant density a change in temperature does not induce any significant variation on the different atomic correlations, and the resulting structure factors are almost identical for different temperatures. The same occurs if the density is fixed to its lower value in equilibrium at 280 K and the temperature of the sample is lowered to 200 K (Figure 5b). However, if at constant temperature (200 K in Figure 5c and 280 K in Figure 5d) the density is decreased from its value in equilibrium at 200 K to that in equilibrium at 280 K, clear variations of the contributions to coherent scattering are observed. All the correlation functions $A_{\alpha\beta}(Q)$ are modified in the low Q range, mainly below 2.5 Å^{-1}. The peaks in this region are shifted toward lower Q values; in addition, the correlations involving carbons and hydrogens experience a rather pronounced increase of intensity in the low-Q region. These effects lead to the observed temperature behavior of the static structure factor, with the global shift of the first peak to lower

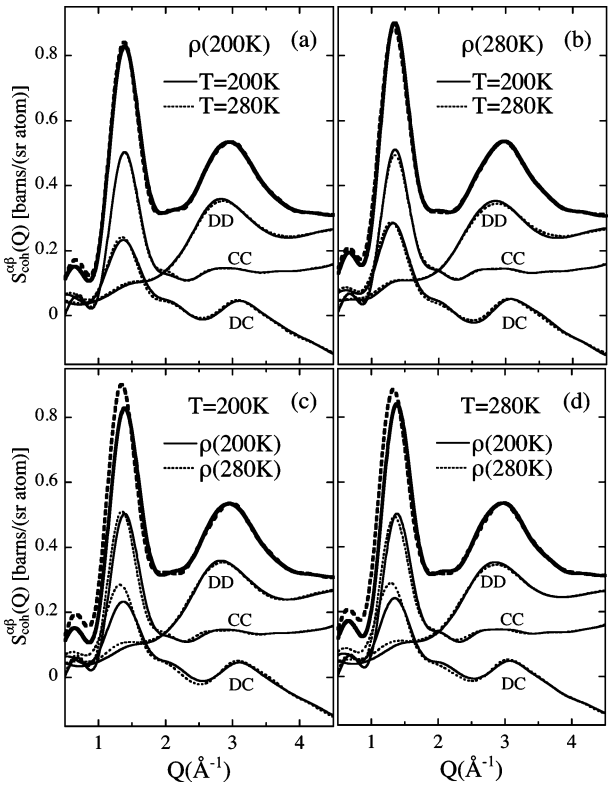

Figure 5. Temperature and density effects on the contributions coming from the different atomic correlations (thin lines) to the structure factor (thick lines) of 1,4-PB at the conditions indicated.

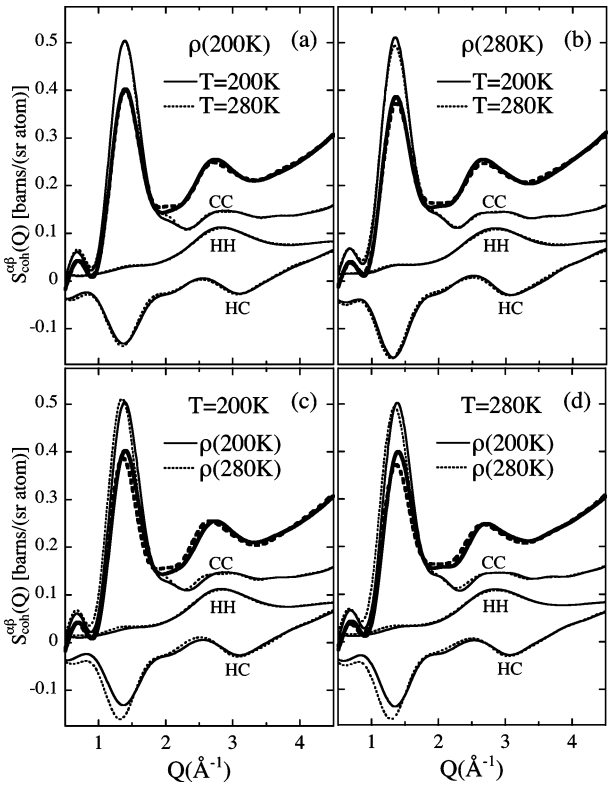

Figure 6. Temperature and density effects on the contributions coming from the different atomic correlations (thin lines) to the partial structure factor (thick lines) of fully protonated 1,4-PB at the conditions indicated.

Q's and the increase of intensity with increasing temperature.[1,3] We note that, though this peak reflects mainly CC correlations, the way it evolves is also strongly influenced by the contributions coming from the mixed term $A_{HC}(Q)$. In a similar way, the partial structure factor of fully protonated polybutadiene is almost insensitive to thermal energy variations for constant density, as can be deduced from Figure 6a,b. The changes induced by varying the density translate however in a different global effect on the coherent intensity. Since the contribution of the mixed term is subtracted in the region $\lesssim 3.5$ Å^{-1}, when the density decreases the increase of the intensity of $A_{HC}(Q)$ in the low-Q flank of its first peak compensates that of the CC correlations contribution in this region, and finally the total intensity remains unchanged below the first maximum (see Figure 6c,d). The intensity in the high-Q flank of the main peak is slightly decreased because of the shift of $S^{CC}_{coh}(Q)$. Thus, in the interplay of the different atomic correlations we have found the natural explanation for the in principle unexpected different temperature dependence of 1,4-PBd6 and 1,4-PBh6 samples and the "anomalous" behavior of 1,4-PBd6. We note that the simulation results suggest also the occurrence of a slight shift also in the second peak of the partial structure factor of the protonated sample. The experimental uncertainties do not allow to confirm such an effect.

We have thus shown that it is the change in density that driving the evolution of the structure factor and the partial structure factor. This result completely agrees with the conclusion drawn by Frick et al.[3] They thoroughly studied the temperature and pressure dependence of the structure factor of this polymer. Moreover, our study on the density dependence of the different correlations allows an interpretation of the pressure dependence experimentally shown by 1,4-PB $S(Q)$.[3,4] We have seen that increasing the density at constant temperature—which is equivalent to increase the hydrostatic pressure—leads mainly to an increase of the intensity in the low-Q flank of the first peak of $A_{HC}(Q)$, together with a small shift of the first peak of $A_{CC}(Q)$ (Figure 5c,d). The resulting effect in $S(Q)$ perfectly agrees with the experimentally observed behavior: only the low-Q part of the peak is shifted with increasing pressure.[4] We note that just the opposite effect should be found for the partial structure factor measured on the protonated sample under pressure, as can be deduced from the density dependence of this function shown in Figure 6c,d. A similar observation was made by Bedrov et al.[20] from their simulations on a united atom model of polybutadiene. In that work, strong shifts of the intermolecular correlations were induced by application of pressure. The reported behavior in that work is qualitatively the same as we observe; however, we note that the effect might appear stronger in that case because larger relative changes in density were considered (about an 8% in comparison with the 5% from this work).

V. Conclusions

This combined study, based on a synergy between neutron diffraction with polarization analysis and fully atomistic MD-simulations, has allowed us to have a deeper insight into the short-range order in 1,4-polybutadiene. A direct comparison between both sets of data, usually not performed in works dealing with simulations, has validated our simulated cell. Moreover, we present for the first time experimental results on the partial structure factor corresponding to the fully

protonated version of this archetypal polymer. Exploiting the information on the simulations, we have found that CC correlations dominate the first diffraction peak for both the deuterated and the protonated samples, while the origin of the second maximum depends on the labeling. Finally, the temperature behavior of the peaks has also been rationalized, arriving at the conclusion that the main role in this game is played by density changes and how they affect mainly the CC correlations and the mixed correlations involving C and H.

Acknowledgment. We thank Dr. L. Willner for the samples. This research project has been supported by the European Commission, NMI3 Contract RII3-CT-2003-505925, and the NoE SoftComp, Contract NMP3-CT-2004-502235. J.C., F.A., and A.A. acknowledge support from the Projects MAT2004-01017 and 9/UPV00206.215-13568/2001, and A.N. acknowledges the FPI grant of the Spanish Ministery of Science and Technology.

References and Notes

(1) Frick, B.; Richter, D.; Ritter, Cl. *Europhys. Lett.* **1989**, *9*, 557.
(2) Buchenau, U.; Monkenbusch, M.; Stamm, M.; Majkrzak, C. F.; Ncker, N. In *Polymer Motion in Dense Systems*; Richter, D.,Springer, T., Eds.; Springer Proceedings in Physics Vol. 29; Springer: Berlin, 1988.
(3) Frick, B.; Alba-Simionesco, C.; Andersen, K. H.; Willner, L. *Phys. Rev. E* **2003**, *67*, 051801.
(4) Cailliaux, A.; Alba-Simionesco, C.; Frick, B.; Willner, L.; Goncharenko, I. *Phys. Rev. E* **2003**, *67*, 010802.
(5) Frick, B.; Richter, D.; Zorn, R.; Fetters, L. J. *J. Non-Cryst. Solids* **1994**, *172*−*174*, 272.
(6) Johnson, J. A.; Saboungi, M.-L.; Price, D. L.; Ansell, S.; Russell, T. P.; Halley, J. W.; Nielsen, B. *J. Chem. Phys.* **1998**, *109*, 7005.
(7) Farago, B.; Arbe, A.; Colmenero, J.; Faust, R.; Buchenau, U.; Richter, D. *Phys. Rev. E* **2002**, *65*, 051803.
(8) Arbe, A.; Moral, A.; Alegría, A.; Colmenero, J.; Pyckhout-Hintzen, W.; Richter, D.; Farago, B.; Frick, B. *J. Chem. Phys.* **2002**, *117*, 1336.
(9) Zorn, R.; Richter, D.; Farago, B.; Frick, B.; Kremer, F.; Kirst, U.; Fetters, L. J. *Physica B* **1992**, *180 & 181*, 534.
(10) Alvarez, F.; Colmenero, J.; Zorn, R.; Willner, L.; Richter, D. *Macromolecules* **2003**, *36*, 238.
(11) Furuya, H.; Mondello, M.; Yang, H.-J.; Roe, R.-J.; Erwin, R. W.; Han, C. C.; Smith, S. D. *Macromolecules* **1994**, *27*, 5674.
(12) Iradi, I.; Alvarez, F.; Colmenero, J.; Arbe, A. *Physica B* **2004**, *350*, e881.
(13) Eilhard, J.; Zirkel, A.; Tschöp, W.; Hahn, O.; Kremer, K.; Schärpf, O.; Richter, D.; Buchenau, U. *J. Chem. Phys.* **1999**, *110*, 1819.
(14) Arrese-Igor, S.; Arbe, A.; Alegría, A.; Colmenero, J.; Frick, B. *J. Chem. Phys.* **2005**, *123*, 014907.
(15) Richter, D.; Monkenbusch, M.; Willner, L.; Arbe, A.; Colmenero, J.; Farago, B. *Europhys. Lett.* **2004**, *66*, 239.
(16) Li, Y.; Mattice, W. L. *Macromolecules* **1992**, *25*, 4942.
(17) Okada, O.; Furuya, H. *Polymer* **2002**, *43*, 971.
(18) Tsolou, G.; Mavrantzas, V. G.; Theodorou, D. N. *Macromolecules* **2005**, *38*, 1478.
(19) Kim, E.-G.; Misra, S.; Mattice, W. L. *Macromolecules* **1993**, *26*, 3432.
(20) Bedrov, D.; Smith, G. D.; Paul, W. *Phys. Rev. E* **2004**, *70*, 011804.
(21) Morton, M.; Fetters, L. J. *Rubber Chem. Technol.* **1975**, *48*, 359.
(22) Lovesey, S. W. *Theory of Neutron Scattering from Condensed Matter*; Clarendon Press: Oxford, 1984.
(23) Squires, G. L. *Introducction to the Theory of Thermal Neutron Scattering*; Dover Publication Inc.: New York, 1996.
(24) Williams, M. G. *Polarized Neutrons*; Oxford University Press: New York, 1988.
(25) Zorn, R. *NIMA* **2002**, *479* 568.
(26) Sun, H. *Macromolecules* **1995**, *28*, 701.
(27) Sun, H.; Mumby, S. J.; Maple, J. R.; Hagler, A. T. *J. Phys. Chem.* **1995**, *99*, 5873.
(28) Sun, H. *J. Phys. Chem. B* **1998**, *102*, 7338.
(29) Sun, H.; Mumby, S. J.; Maple, J. R.; Hagler, A. T. *J. Phys. Chem. B* **1998**, *102*, 7338.
(30) Theodorou, D. N.; Suter, U. W. *Macromolecules* **1986**, *19*, 139.
(31) Theodorou, D. N.; Suter, U. W. *Macromolecules* **1986**, *19*, 379.
(32) Colmenero, J.; Arbe, A.; Alvarez, F.; Narros, A.; Monkenbusch, M.; Richter, D. *Europhys. Lett.* **2005**, *71*, 262.

MA051466A